Draft version November 13, 2021
Typeset using LaTeX **twocolumn** style in AASTeX62

Updated High-Temperature Opacities for the Dartmouth Stellar Evolution Program

Thomas M. Boudreaux,[1] Brian C. Chaboyer,[1] and Gregory A. Feiden[2]

[1] *Department of Physics and Astronomy, Dartmouth College, Hanover, NH 03755, USA*
[2] *Department of Physics and Astronomy, University of North Georgia, GA 30597, USA*

ABSTRACT

The equations of stellar structure have proven astonishingly predictive when describing stars interior structures. In their most basic form they constitute 4 ordinary, first-order, differential equations. However, they are not on their own well enough constrained to solve. In addition to the four ODEs, an equation of state, thermal conductivities, nuclear reaction rates, and opacities are all required when modeling a star. Some of these additional constraints can be computed on the fly; however, as yet there is no effective way to compute opacities at run time. Rather, stellar structure programs use pre-tabulated opacities over a range of temperatures, densities, and chemical compositions. The Dartmouth Stellar Evolution Program (DSEP) has used OPAL opacities for the last decade and a half; however, there are now more up to date elemental opacity tables from OPLIB. Moreover, OPAL opacities can no longer be reliably generated for different chemical compositions. Here we present an overview of how we update DSEP to use opacities from OPLIB in addition to preliminary results from two studies making use of these updated opacities.

1. INTRODUCTION

Over the last half of the 19th and first decade of the 20th centuries Lane, Ritter, and Emden codified the earliest mathematical model of stellar structure, the polytrope (Equation 1), in *Gaskugeln* (Gas Balls) (Emden 1907).

$$\frac{d}{d\xi}\left(\xi^2\frac{d\theta}{d\xi}\right) = -\xi^2\theta^n \tag{1}$$

Where ξ and θ are dimensionless parameterizations of radius and temperature respectively, and n is known as the polytropic index. Despite this early work, it wasn't until the late 1930s and early 1940s that the full set of equations needed to describe the structure of a steady state, radially-symmetric, star (known as the equations of stellar structure) began to take shape as proton-proton chains and the Carbon-Nitrogen-Oxygen cycle were, for the first time, seriously considered as energy generation mechanisms (Cowling 1966). Since then, and especially with the proliferation of computers in astronomy, the equations of stellar structure have proven themselves an incredibly predictive set of models.

There are currently many stellar structure codes (e.g. Dotter et al. 2008; Kovetz et al. 2009; Paxton et al. 2011) which integrate the equations of stellar structure — in addition to equations of state and lattices of nuclear reaction rates — over time to track the evolution of an individual star. The Dartmouth Stellar Evolution Program (DSEP) (Chaboyer et al. 2001; Bjork & Chaboyer 2006; Dotter et al. 2008) is one such, well tested, stellar evolution program.

DSEP solves the equations of stellar structure using the Henyey method (Henyey et al. 1964). This is a relaxation technique making use of a Newton–Raphson root finder and therefore requires some initial guess to relax towards a solution. This guess will be either some initial, polytropic, model or the solution from the previous timestep. In order to evolve a model through time DSEP alternates between solving for reaction rates and the structure equations. At some temperature and pressure from the solution to the structure equations DSEP finds the energy generation rate due to proton-proton chains, the CNO cycle, and the tripe-alpha process from known nuclear cross sections. These reaction rates yield both photon and neutrino luminosities as well as chemical changes over some small time step. Thermodynamic variables are calculated using an equation of state routine which is dependent on the initial model mass. All the updated physical quantities (pressure, luminosity, mean molecular mass, temperature) are then used to solve the structure equations again. This process of using a solution to the structure equations to calculate reaction rates which then inform the next structure solution continues until DSEP can no longer find a solution. This can happen as the stellar structure equations

are extremely stiff. In addition, for finite radial mesh sizes, discontinuities can occur.

While other stellar evolution programs, such as the widely used Modules for Experimentation in Stellar Astrophysics (MESA) (Paxton et al. 2011), consider a more complex handling of nuclear reaction rate calculations, and are consequently more applicable to a wider range of spectral classes than DSEP, DSEP has certain advantages over these other programs that make it well suited for certain tasks, such as low-mass modeling. For one, DSEP generally can evolve models much more rapidly than MESA and has a smaller memory footprint while doing it. This execution time difference is largely due to the fact that DSEP makes some simplifying assumptions due to its focus only on models with initial masses between 0.1 and 5 $M_\odot$ compared to MESA's more general approach. Moreover, MESA elects to take a very careful handling of numeric uncertainty, going so far as to guarantee byte-to-byte similarity of the same model run on different architectures (Paxton et al. 2011). DSEP on the other hand makes no such guarantee. Rather, models evolved using DSEP will be accurate down to some arbitrary, user controllable, tolerance but beyond that point may vary from one computer to another. Despite this trade off in generality and precision, the current grid of isochrones generated by DSEP (Dotter et al. 2008), has been heavily cited since its initial release in 2008, proving that there is a place for a code as specific as DSEP.

As DSEP pushes a star along its evolutionary track the radiative opacity must be known for a wide range of temperatures, pressures, and compositions. Specifically, opacity is a key parameter in the equation of energy transport. With current computational tools it's infeasible to compute opacities on the fly; rather, Rossland Mean opacity (κ_R) for individual elements must be pre-tabulated over a wide range of temperatures and densities. These opacities can then be somewhat arbitrarily mixed together and interpolated to form opacity lookup-tables. Multiple groups have preformed these calculations and subsequently made tables available to the wider community, these include the Opacity Project (OP Seaton et al. 1994), Laurence Livermore National Labs OPAL opacity tables (Iglesias & Rogers 1996), and Los Alamos National Labs OPLIB opacity tables (Colgan et al. 2016).

The OPAL opacity tables in particular are very widely used by current generation stellar evolution programs (in addition to current generation stellar model and isochrone grids). However, they are no longer the most up date elemental opacities. Moreover, the generation mechanism for these tables, a webform, is no longer reliably online. Consequently, it makes sense to transition to more modern opacity tables with a more stable generation mechanism.

Here we will present work transitioning DSEP from OPAL opacities to opacities based on measurements from Los Alamos national Labs T-1 group (OPLIB Colgan et al. 2016). Moreover, we will present two projects which are in large part reliant on these updated opacities. For the first project we investigate the affects of chemically self consistent modeling of multiple populations within the globular cluster NGC 2808, and for the second project we present the effects of the OPLIB opacities on the location of the recently discovered Gaia M-dwarf gap.

This paper is organized as follows. In Section 2 we outline some basic information about OPLIB opacities, how we query them, and how we modify them to work with DSEP. In Section 3 we discuss scientific background of the first project along with the current work done towards its goal. Finally, in Section 4 we present our findings on the effects of OPLIB opacities on the location of the Gaia M-dwarf gap.

2. OPACITIES

Radiative opacity is fundamental to stellar structure, it determines how much incident radiation is absorbed or scattered. Moreover, when a media is in thermodynamic equilibrium with the radiation field, that is when the temperature of the media and that of the radiation field is the same, the opacity may be used via Kirchhoff's law to find the emissivity of a material (Huebner & Barfield 2014). Local Thermodynamic Equilibrium (LTE) is a common state to find within a star and therefore stellar models have long relied on opacities calculated in LTE.

2.1. *OPLIB Opacities*

Los Alamos National Labs OPLIB opacity tables were first computed in the 1990s using the LEDCOP code (Magee et al. 1995); however, since 2004 efforts have been underway to shift OPLIP from LEDCOP to ATOMIC (Magee et al. 2004). ATOMIC is a LTE and non-LTE opacity and plasma modeling code. A major strength of ATOMIC when compared to the older LEDCOP is its ability to vary its refinement level (Fontes et al. 2015). For a more detailed breakdown of how the most up-to-date set of OPLIB tables are generated see (Colgan et al. 2016).

The most up to date OPLIB tables include monochromatic Rosseland mean opacities for elements hydrogen through zinc over temperatures 0.5eV to 100 keV and for mass densities from approximately 10^{-8} g cm^{-3} up to approximately 10^4 g cm^{-3} (though the exact mass

density range varies as a function of temperature). The Rosseland mean opacity as reported in OPLIB tables is given in Equation 2.

$$\frac{1}{\kappa_R} = \frac{\int_0^\infty \frac{1}{\kappa_\nu} n_\nu^3 \frac{\partial B_\nu}{\partial T} d\nu}{\int_0^\infty \frac{\partial B_\nu}{\partial T} d\nu} \tag{2}$$

Here, B_ν is the Planck function, n_ν is the frequency-dependent refractive index (Armstrong et al. 2014), and κ_ν is the frequency-dependent opacity. κ_ν is defined as the sum of the bound-bound, bound-free, free-free, and scattering opacity computed by ATOMIC.

2.2. *Table Querying and Conversion*

DSEP uses pre-computed high-temperature opacity tables, in the format supplied by OPAL. These tables list the Rosseland-mean opacity, κ_R, along three dimensions: temperature, a density proxy R, and composition. R is defined as

$$R = \frac{\rho}{T_6^3} \tag{3}$$

Where $T_6 = T \times 10^{-6}$ and ρ is the mass density. If T and ρ are given in cgs then for much of the radius of a star $\log(R) \sim -1.5$. The reason DSEP uses R as opposed to simply tracking opacity over density is that R stays relatively fixed, whereas there is an enormous dynamic range of densities within a star ($\sim 10^5$ [g cm^{-3}] at the core of an RGB star all the way down to $\sim 10^{-8}$ [g cm^{-3}] within the envelope). This reduction in dynamic-range is important to help reduce floating-point numeric errors, which ends up being the primary motivation to use R over ρ.

OPLIB high-temperature opacity tables will replace the OPAL tables DSEP has used since the release of the Dartmouth Stellar Evolution Database (DSED) in 2008 (Dotter et al. 2008). Just as OPAL tables were, OPLIB tables are queried from a web interface[1]. So that we might generate many tables easily and quickly we develope a web scraper built with Python's `requests` module in addition to the 3rd party `mechanize` and `BeautifulSoup` modules (Chandra & Varanasi 2015; Richardson 2007) which can get tables with minimal human intervention. This web scraper submits a user requested chemical composition (composed of mass fractions for elements from Hydrogen to Zinc) to the Los Alamos web form, selects 0.0005 keV as the lower temperature bound and 60 keV as the upper temperature bound, and finally requests opacity measurements for 100 densities, ranging from $1.77827941 \times 10^{-15}$ [g cm^{-3}] up to 1×10^7 [g cm^{-3}], at each temperature interval. These correspond to approximately the same temperature and density range of opacities present in the OPAL opacity tables.

So as not to break compatibility with OPAL tables we create a translation layer to convert OPLIB tables to OPAL format. This allows for transparent use of the new tables without any direct modifications to the DSEP source. The primary job of this translation layer is to unit conversion, secondarily the structure of OPAL tables must be matched byte-for-byte.

OPLIB reports κ_R as a function of mass density, temperature in keV, and composition. Recall that OPAL tables present opacity as a function of temperature in Kelvin, R, and composition. The conversion from temperature in keV to Kelvin is trivial

$$T_K = T_{keV} * 11604525.0061657 \tag{4}$$

The conversion from mass density to R is more involved. Because R is coupled with both mass density and temperature there there is no way to directly convert tabulated values of opacity reported in the OPLIB tables to their equivalents in R space. Instead we must rotate the tables, interpolating $\kappa_R(\rho, T_{eff}) \rightarrow \kappa_R(R, T_{eff})$.

As a first step in this rotation we use the `interp2d` function within `scipy`'s `interpolate` (Virtanen et al. 2020) module to construct a cubic bivariate B-spline (DIERCKX 1981) interpolating function s, with a smoothing factor of 0, representing the surface $\kappa_R(\rho, T_{eff})$. For each R^i and T_{eff}^j which DSEP expects high-temperature opacities to be reported for, we evaluate Equation 3 to find $\rho^{ij} = \rho(T_{eff}^j, R^i)$. Opacities in T_{eff}, R space are then inferred as $\kappa_R^{ij}(R^i, T_{eff}^j) = s(\rho^{ij}, T_{eff}^j)$. Finally, some number of upper-left and lower-right hand entries in each table are discarded as DSEP takes non rectangular tables as input, the exact number and indices of the discarded entries is dependent on composition.

As first-order validation of this interpolation scheme we can preform a similar interpolation in the opposite direction, rotating the tables back to $\kappa_R(\rho, T_{eff})$ and then comparing the initial, "raw", opacities to those which have gone through the interpolations process. Figure 1 shows the fractional difference between the raw opacities and a set which have gone through this double interpolation. The red line denotes $Log(R) = -1.5$ where models will tend to sit for much of their radius. Along the $Log(R) = -1.5$ line the mean fractional difference is $\langle\delta\rangle = 0.006$ with an uncertainty of $\sigma_{\langle\delta\rangle} = 0.009$. One point of note is that, because the initial rotation into $Log(R)$ space also reduces the domain of the opacity

[1] https://aphysics2.lanl.gov/apps/

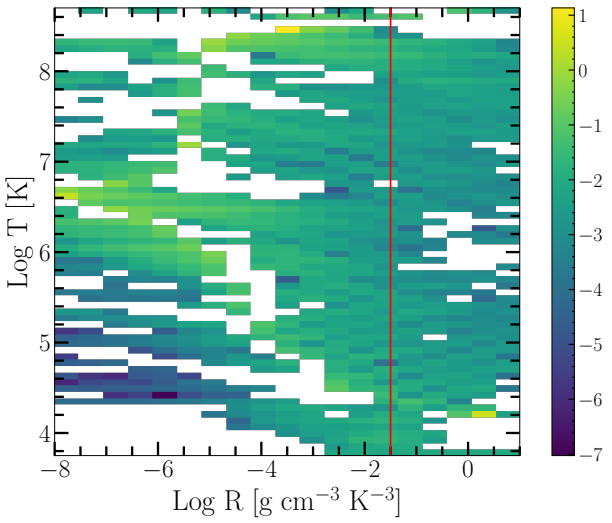

Figure 1. Log Fractional Difference between opacities in $\kappa_R(\rho, T_{eff})$ space directly queried from the OPLIB webform and those which have been interpolated into $Log(R)$ space and back. Note that, due to the temperature grid DSEP uses not aligning perfectly which the temperature grid OPLIB uses there may be edge effects where the interpolation is poorly constrained. The red line corresponds to $Log(R) = -1.5$ where much of a stellar model's radius exists.

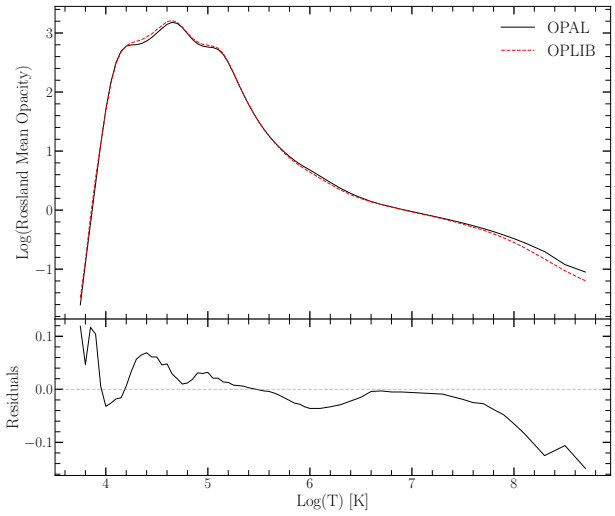

Figure 2. Rosseland mean opacity with the GS98 solar composition for both OPAL opacities and OPLIB opacities (top). Residuals between OPLIB opacities and OPAL opacities (bottom). These opacities are plotted at $\log_{10}(R) = -1.5$, $X = 0.7$, and $Z = 0.02$.

function interpolation-edge effects which we avoid initially by extending the domain past what DSEP needs cannot be avoided when interpolating back into ρ space. In future, a more robust validation, which does not reduce the domain size will be conducted.

2.3. *Opacity Validation*

In order to further validate the OPLIB high-temperature opacities we first visually compare a set of opacity vs. temperature curves from OPLIB at a constant R and Grevesse & Sauval (1998) composition (GS98) to the same curve from OPAL. A characteristic opacity vs temperature curve is shown in Figure 2, $\log_{10}(R) = -1.5$ is chosen as for much of the radius of a main sequence star $\log_{10}(R)$ is around that value. The largest variation in κ_R from OPAL to OPLIB at $\log_{10}(R) = -1.5$ is on the order of a few percent. This is inline with expectations of OPLIB and OPAL being in relatively close agreement (Colgan et al. 2016).

To further validate the OPLIB opacities we generate a solar calibrated stellar model (SCSM) using the new tables. SCSMs are generally models where some initial parameters have been iteratively adjusted to minimize some loss function between that models output parameters and the observed values of those parameters for the Sun. In the context of this paper we adjust both the convective mixing length parameter, α_{ML}, and the initial Hydrogen mass fraction, X, to minimize the difference between the models final radius and luminosity and that of the sun.

Optimization of α_{ML} and X is done with a quite naive gradient descent algorithm. For each optimization step three models are evolved: a reference model, a model with a small perturbation to the hydrogen mass fraction but the same mixing length as the reference model, and a model with a small perturbation to the mixing length but the same hydrogen mass fraction as the reference. Perturbations are sampled from a normal distribution (implemented though `numpy.random`) with scale set to an adjustable parameter, η. This distribution is sampled and that sample is then added to the reference value for either X or α_{ML}. The luminosity and radius of the three evolved models are compared to solar values and the gradient of the resultant $L - L_\odot$, $R - R_\odot$ surface is followed down to new estimates for the reference values of X and α_{ML}. This process is is repeated until the difference between successive X and α_{ML} drops below one part in 10^5.

If we generate a SCSM using the GS98 OPAL opacity tables we find a best estimate of $X = 0.7066$ and $\alpha_{ML} = 1.9333$. When we preform the same calibration but substituting in the GS98 OPLIB tables we find $X = 0.7107$ and $\alpha_{ML} = 1.9629$. This represents $\sim 0.5\%$ difference in the SCSM hydrogen mass fractions and $\sim 1.5\%$ change in the SCSM convective mixing length parameters when comparing models using OPAL and OPLIB tables. An HR-diagram for the two calibrated models is presented in Figure 3. While the two evolutionary tracks are very similar, note that the OPLIB

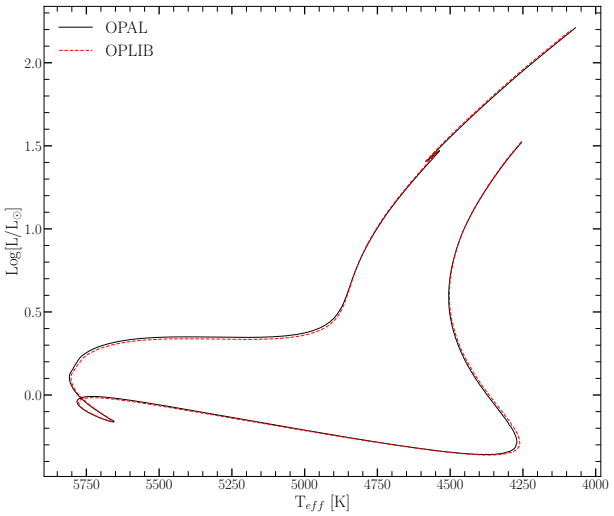

Figure 3. HR Diagram for the two SCSMs, OPAL and OPLIB. OPLIB is show as a grey dashed line.

SCSM's luminosity is systematically lower at the same effective temperature all the way from the premain sequence up and until the star leaves the main sequence, at which point it is effectively the same as the OPAL SCSM. This luminosity difference between OPAL and OPLIB based models is consistent with expectations given the differences in opacities. Opacity is of primary importance only in radiative regions of a star ($\gtrsim 10^6$ K). Figure 2 shows that OPLIB opacities are uniformly lower than OPAL opacities above 10^6 K. These lower opacities will steepen the temperature gradient within the stellar model as radiation streams more freely outward.

3. MULTIPLE POPULATIONS IN NGC 2808

Globular clusters (GC, Herschel 1814) are among the oldest groupings of stars in the Universe, with typical ages greater than 10 Gyr. They are characterized by their compact size — typical half-light radius < 10 pc but up to 10s of pc — and high surface brightness — $M_V \sim -7$. Traditionally, GCs were believed to contain a single stellar population, much like open clusters. However, chemical inhomogeneities in GCs have been known about since the early 1970s (e.g. Osborn 1971) and by the late 1980s multiple clusters were known which exhibited features in their CMDs consistent with either bimodal or multimodal stellar populations (e.g. Norris 1987).

Whereas, people have have often tried to categorized objects as GCs by making cuts along half-light radius, density, and surface brightness profile, in fact many objects which are generally thought of as GCs don't cleanly fit into these cuts. Consequently, Carretta et al. (2010) proposed a definition of GC based on observed chemical inhomogeneities in their stellar populations. The modern understanding of GCs then is not simply one of a dense cluster of stars which may have chemical inhomogeneities and multiple populations; rather, it is one where those chemical inhomogeneities and multiple populations themselves are the defining element of a GC.

Variations in observed abundances were initially attributed to evolutionary mixing (Denisenkov & Denisenkova 1990). However, enhanced abundances are still observed in scarcely evolved main sequence stars, ruling out evolutionary mixing as the primary mechanism (Gratton et al. 2004; Briley et al. 2004). Moreover, mixing of a degree high enough to explain the observed anomaly in cyanogen abundances would result in extended lifetimes and a broadened main sequence turn off region in the CMD of ancient GCs, which is not observationally supported. More recently, precision Hubble photometry revealed that almost every cluster in orbit of the milky way comprises multiple main sequences (Piotto et al. 2007; Roh et al. 2011; Milone et al. 2012) (MMP) as opposed to a single stellar population (SP).

Single stellar populations had been assumed due to spectroscopically uniform iron abundances (Gratton et al. 2012) and very narrow principal sequences (Stetson & Harris 1988), both of which are indicative of a single stellar population. The first conclusive evidence for MMPs came with Hubble Space Telescope (HST) high precision crowded field photometry in which three distinct main sequences in NGC 2808 were identified (Piotto et al. 2007). Since this discovery, split main sequences have been found in nearly all Milky Way globular clusters studied by HST (Anderson et al. 2009; Milone et al. 2012). Split stellar populations are believed to be due to enhanced helium abundances in the stellar populations formed after the primordial population of stars (D'Antona et al. 2005; Piotto et al. 2007). When compared to primordial helium mass fractions (Y) of $Y \sim 0.25$ (Collaboration et al. 2016) or solar helium abundances $Y \sim 0.27$ (Vinyoles et al. 2017) these populations have mass fractions as high as $Y \sim 0.4$. Helium enhancement is strongly suspected to be the result of an earlier, more massive population dying off, enriching the interstellar medium (Gratton et al. 2001, 2004, 2012). The primary open question then is not why some populations are enhanced in helium; rather, it is to what extent they are enhanced.

Due to the relatively high and tight temperature range of partial ionization for helium it cannot be observed in globular clusters; consequently, the evidence for these enhanced helium abundances originates from comparison of theoretical stellar isochrones to the observed color

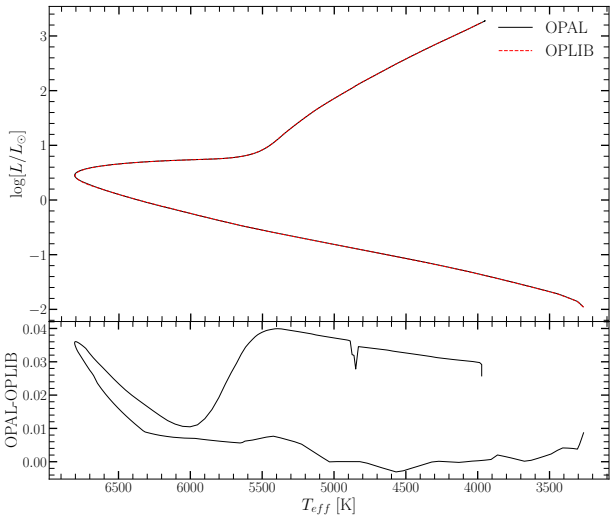

Figure 4. 10 Gyr & Y=0.33 isochrones for models generated with OPAL and OPLIB opacities tables (top). Residuals between isochrones (bottom).

magnitude diagrams of globular clusters. None of the isochrones used to date in these comparison have been generated from models with self consistent chemistries.

3.1. *Population Opacities*

Given the relative historic difficulty in generating new opacity tables, stellar models have tended to use opacity tables whos range of compositions is derived from simple rescaling of the some solar composition. Here we use our OPLIB web scraper to generate opacity tables with compositions specific to each population in NGC 2808.

These population have been studied in depth by Feiden and their chemical compositions were determined in Milone et al. (2015) (see Table 2 in that paper). While we cannot currently make fully self-consistent models due to still ongoing atmospheric modeling, we can make a first pass investigation of the affect of OPLIB opacities (Figure 4). Note how the models generated using OPLIB opacity tables have a systematically lower luminosity. Recall, that this is consistent with the overall lower opacities of the OPLIB tables.

3.2. *Additional Consistency*

The lack of self consistency presents problems at other stages of stellar evolution codes. Perhaps most importantly, where the interior of a stellar model meets the atmosphere. Atmospheric models such as a grey (Eddington 1916), Krishna Swamy (Krishna Swamy 1966), or Phoenix (Husser et al. 2013) model atmosphere provide one pressure boundary conditions to solve the two-point boundary value problem that is the equations of stellar structure. Once again however, models tend to use atmospheres with non consistent chemistries. Therefore, one key element of NGC 2808 modeling is the incorporation of new atmospheric models, generated from the MARCS grid of model atmospheres (Plez 2008), which match interior elemental abundances. Members of our collaboration are currently working on such atmospheric modeling.

Finally, The isochrones used to infer the degree of helium enhancements assume that convection operates in the same manner in metal-poor stars as it does in the Sun. However, observations from *Kepler* of metal-poor red giants (Bonaca et al. 2012; Tayar et al. 2017), in concert with interferometric radius determination of the metal-poor sub-giant HD 140283 (Creevey et al. 2015), have shown that the efficiency of convection changes with iron content. We will additionally modify DSEP to capture this variation in convective efficiency. While we wait for atmospheric modeling to be completed it makes sense to investigate other locations where opacity differences on the order of 5% may affect results.

4. GAIA M-DWARF GAP

Due to initial mass requirements of the molecular clouds which collapse to form stars, star formation is strongly biased towards lower mass, later spectral class, stars when compared to higher mass stars. Partly as a result of this bias and partly as a result of their extremely long main-sequence lifetimes, M-dwarfs make up approximately 70 percent of all stars in the galaxy. Moreover, some planet search campaigns have focused on M-dwarfs due to the relative ease of detecting small planets in their habitable zones (e.g. Nutzman & Charbonneau 2008). M-dwarfs then represent both a key component of the galactic stellar population as well as the possible set of stars which may host habitable exoplanets. Given this key location M-dwarfs occupy in modern astronomy it is important to have a thorough understanding of their structure and evolution.

4.1. *Observations and Instability*

Gaia Data Release 2 (DR2) revealed a previously unknown structure in in the $G_{\rm BP} - G_{\rm RP}$, M_G color-magnitude diagram (Figure 5) corresponding to stars with a mass near that where a star transitions from fully convective to having both convective and radiative regions within (the fully convective transition mass) (Jao et al. 2018). The so called Gaia M-dwarf gap, or Jao gap, represents a decrease in luminosity and commensurately a decrease in stellar density — by approximately 17% — over this mass range. Jao et al. (2018); Baraffe & Chabrier (2018) suggest that this density deficiency is due to stars between a mass of 0.3 to 0.35 $M_\odot$ transitioning into full convectivity.

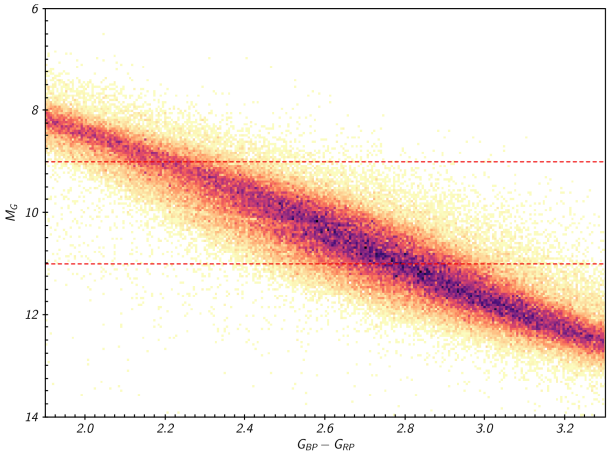

Figure 5. Figure 1 from Jao et al. (2018) showing the so called "Jao Gap" at $M_G \approx 10$

A theoretical explanation for such a density deficiency comes from van Saders & Pinsonneault (2012), who propose that directly above the transition mass between a star with a radiative core and convective envelope and a fully convective star, due to asymmetric production and destruction of He^3 during the proton-proton I chain (ppI), periodic luminosity variations can be induced. This process is known as convective-kissing instability. Take for example a star with a mass right on the fully convective transition. Such a star will descent the pre-MS with a radiative core; however, as the star reaches the zero age main sequence (ZAMS) and as the core temperature exceeds 7×10^6 K, enough energy will be produced by the ppI chain that the core becomes convective. At this point the star exists with both a convective core and envelope, in addition to a thin, radiative, layer separating the two. At this Point asymmetries in ppI affect the evolution of the stars convective core.

The proton-proton I chain constitutes three reactions

1. $p + p \longrightarrow d + e^+ + \nu_e$
2. $p + d \longrightarrow {}^3\mathrm{He} + \gamma$
3. ${}^3\mathrm{He} + {}^3\mathrm{He} \longrightarrow {}^3\mathrm{He} + 2p$

Because reaction 3 of ppI consumes ^{3}He at a slower rate than it is produced by reaction 2, ^{3}He abundance increases in the core increasing energy generation. The core convective zone will therefore expand as more of the star becomes unstable to convection. This expansion will continue until the core connects with the convective envelope. At this point convective mixing can transport material throughout the entire radius of the star and the high concentration of ^{3}He will rapidly diffuse outward, away from the core, again decreasing energy generation as reaction 3 slows Down. Ultimately, this leads to the convective region around the core pulling back away from the convective envelope, leaving in place the radiative transition zone, at which point ^{3}He concentrations build up in the until it once again expands to meet the envelope. This process repeats until chemical equilibrium is reached throughout the star and the core can sustain high enough nuclear reaction rates to maintain contact with the envelope, resulting in a fully convective star.

4.2. *Modeling the Gap*

Since the identification of the Gaia M-dwarf gap, stellar modeling has been conducted to better constrain its location, effects, and exact cause (e.g. Mansfield & Kroupa 2021; Feiden et al. 2021). When modeling the gap manifests as a discontinuity in the mass-luminosity relation. However, all modeling of the gap has been done using GS98 OPAL high-temperature opacities. This presents similar issues to the use of these tables when modeling multiple populations in GCs; namely, OPAL tables are no longer the most up to date in their component opacities .

Mansfield & Kroupa (2021) and Feiden et al. (2021) identify that the gap's mass location is correlated with model metallicity — the mass-luminosity discontinuity in lower metallicity models being at a commensurately lower mass. Feiden et al. (2021) suggests this dependence is due to the steep relation of the radiative temperature gradient, ∇_{rad}, on temperature and in turn, on stellar mass.

$$\nabla_{rad} \propto \frac{L\kappa}{T^4} \tag{5}$$

As metallicity decreases so does opacity, which, by Equation 5, dramatically lowers the temperature where radiation will dominate energy transport (Chabrier & Baraffe 1997). Since main sequence stars are virialized the core temperature is proportional to the core density and total mass (Equation 6). Therefore, if the core temperature where convective-kissing instability is expected decreases with metallicity, so to will the mass of stars which experience such instabilities.

$$T_c \propto \rho_c M^2 \tag{6}$$

4.3. *Consistently Modeling the Gap*

In order to address the two main issues with using OPAL opacity tables we use our OPLIB opacity table web scraper to generate a set of tables that consistently model lower metallicities. Specifically, we generate tables for $Z_\odot = 0.017$, $Z = 0.01$, $Z = 0.001$, and

$Z = 0.0001$. Compositions are derived from the GS98 solar composition, with the mass fractions between metals remaining constant, and only the total metal mass fraction is allowed to vary. Moreover, Helium mass fraction is held constant as extra mass from the reduced metallicity is put into additional Hydrogen.

For each metallicity 101, uniformly spaced, models from 0.3 to 0.5 $M_\odot$ (spacing of 0.001 $M_\odot$) are evolve with both the GS98 OPAL opacity table and OPLIB tables, hereafter these are the "coarse" models. For each set of coarse models the discontinuity in the mass-luminosity relation is identified at an age of 7 Gyr (Figures 6 & 7 shows a characteristic example).

Immediately, the difference in mass where the discontinuity manifests is clear. For each metallicity the discontinuity in the OPLIB models is approximately one one-hundredth of a solar mass lower than the discontinuity in the OPAL models. We can validate that this discontinuity is indeed correlated with the convective transition mass; Figure 8 shows an example of the model forming radiative zones at approximately the same masses where the discontinuity in the mass-luminosity function exists.

At this resolution only a few models exist within the mass range of the discontinuity. In order to better constrain its location we run a series of "fine" models, with a mass step of 0.0001 $M_\odot$ and ranging from where the mass derivative first exceeds two sigma away from the mean derivative value up to the mass where it last exceeds two sigma away from the mean. A characteristic fine mass-luminosity relation is shown in Figure 9.

Using the fine models we identify the location of the discontinuity in the same manner as before, results of this are presented in Table 1. Of note with the mass ranges we measure for the discontinuity is that are generally not in agreement with those measured in Mansfield & Kroupa (2021). However, the luminosity difference from over the gap ($\approx 0.1 mag$) is similar to both the observational difference and that reported in Mansfield & Kroupa (2021). Currently, it is not clear why our mass range is not in agreement with the Mansfield & Kroupa (2021) mass range and further investigation is therefore needed.

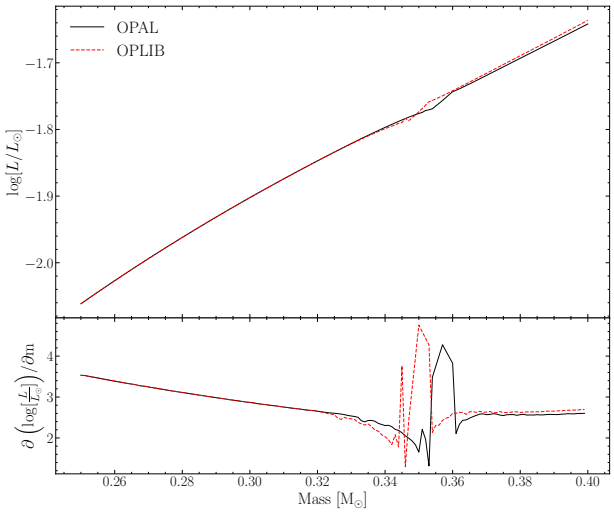

Figure 6. Mass-Luminosity relation for Z=0.01 at 7 Gyr for models run with both OPAL and OPLIB high-temperature opacity tables and a mass step between them of 0.001 $M_\odot$ (top). Derivative of luminosity with respect to mass for the OPAL and OPLIB models (bottom).

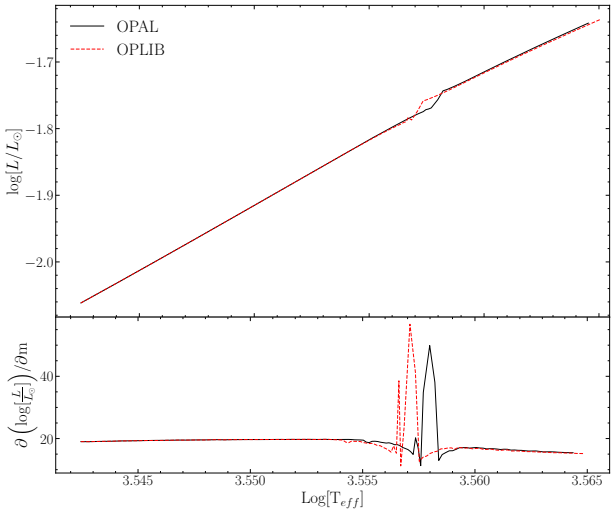

Figure 7. Temperature-Luminosity relation for Z=0.01 at 7 Gyr for models run with both OPAL and OPLIB high-temperature opacity tables and a mass step between them of 0.001 $M_\odot$ (top). Derivative of the luminosity with respect to the temperature for the OPAL and OPLIB models (bottom)

5. CONCLUSION

Here we have presented updated opacity tables for use with the Dartmouth Stellar Evolution Program. These new tables come from the most recent ATOMIC release of OPLIB. Models evolved using OPLIB opacity tables yield solar calibrated hydrogen mass fractions within 0.5% of those from models evolved with OPAL tables and calibrated convective mixing lengths within 1.5% of OPAL models.

Additionally, we present two projects which will make use of these updated opacities. One, is just getting underway but will eventually produce the first self consistently models of He enhancement across the multiple stellar populations of NGC 2808. The second demonstrates that the location of the Gaia M-dwarf gap is sensitive to opacity and that models using OPLIB opac-

$Z =$	$Z_\odot$	0.01	0.001	0.0001
OPAL	0.3803 - 0.384	0.3583 - 0.3631	0.34 - 0.3448	0.362 - 0.3663
OPLIB	0.374 - 0.3767	0.3526 - 0.3567	0.3358 - 0.3406	0.3577 - 0.3621

Table 1. Mass ranges for the discontinuity in OPAL and OPLIB models. Masses are given in solar masses.

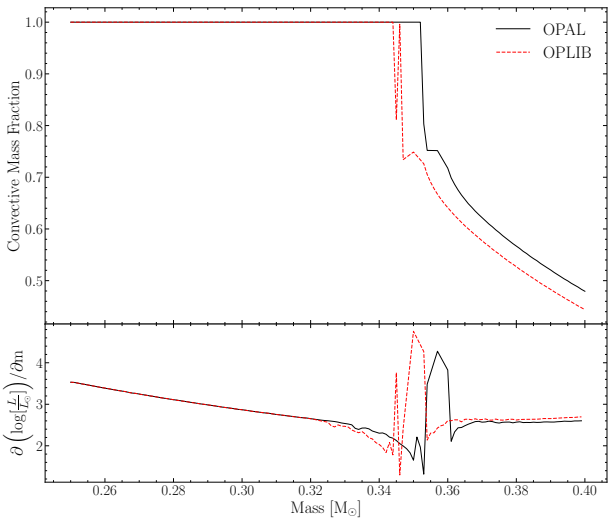

Figure 8. Convective Mass Fraction vs. initial model mass for Z=0.01 at 7 Gyr (top), Derivative of luminosity with respect to mass for the OPAL and OPLIB models (bottom). Note how the model transitions from fully convective at approximately the same mass where the discontinuity exists.

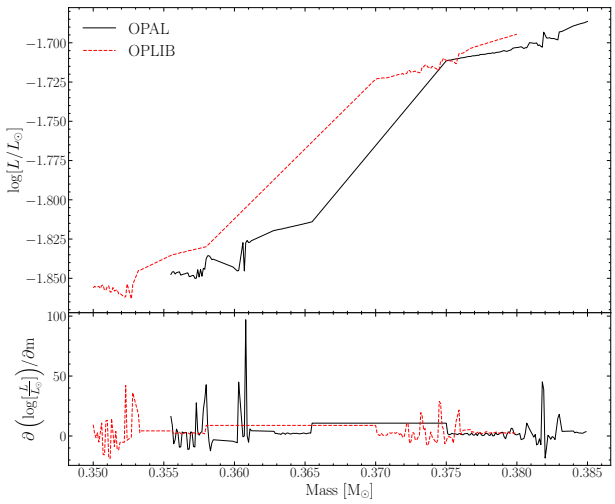

Figure 9. Mass-Luminosity relation for Z=0.01 at 7 Gyr for models run with both OPAL and OPLIB high-temperature opacity tables and a mass step between them of 0.0001 $M_\odot$ (top). Derivative of luminosity with respect to mass for the OPAL and OPLIB models (bottom).

ities manifest the mass-luminosity discontinuities at consistently lower masses than models using OPAL opacities do. We hope that in future the ability to quickly generate arbitrary high-temperature opacity tables will encourage more studies to maintain chemical self consistence.

This research has made use of NASA's astrophysical data system (ADS). We acknowledge the support of an NASA grant (No. 80NSSC18K0634). Additionally, we would like to thank James Colgan for his assistance with the OPLIB opacity tables. We would like to thank Aaron Dotter, and Elisabeth Newton for their assistance. Finally, we thank our colleagues and peers in for their continuing and appreciated support.

REFERENCES

Anderson, J., Piotto, G., King, I., Bedin, L., & Guhathakurta, P. 2009, The Astrophysical Journal Letters, 697, L58

Armstrong, G. S. J., Colgan, J., Kilcrease, D. P., & Magee, N. H. 2014, High Energy Density Physics, 10, 61, doi: 10.1016/j.hedp.2013.10.005

Baraffe, I., & Chabrier, G. 2018, A&A, 619, A177, doi: 10.1051/0004-6361/201834062

Bjork, S. R., & Chaboyer, B. 2006, ApJ, 641, 1102, doi: 10.1086/500505

Bonaca, A., Tanner, J. D., Basu, S., et al. 2012, The Astrophysical Journal Letters, 755, L12, doi: 10.1088/2041-8205/755/1/L12

Briley, M. M., Cohen, J. G., & Stetson, P. B. 2004, The Astronomical Journal, 127, 1579

Carretta, E., Bragaglia, A., Gratton, R. G., et al. 2010, Astronomy & Astrophysics, 516, A55

Chaboyer, B., Fenton, W. H., Nelan, J. E., Patnaude, D. J., & Simon, F. E. 2001, ApJ, 562, 521, doi: 10.1086/323872

Chabrier, G., & Baraffe, I. 1997, A&A, 327, 1039. https://arxiv.org/abs/astro-ph/9704118

Chandra, R. V., & Varanasi, B. S. 2015, Python requests essentials (Packt Publishing Ltd)

Colgan, J., Kilcrease, D. P., Magee, N. H., et al. 2016, in APS Meeting Abstracts, Vol. 2016, APS Division of Atomic, Molecular and Optical Physics Meeting Abstracts, D1.008

Collaboration, P., et al. 2016, XIII. Cosmological parameters

Cowling, T. G. 1966, QJRAS, 7, 121

Creevey, O., Thévenin, F., Berio, P., et al. 2015, Astronomy & Astrophysics, 575, A26

Denisenkov, P. A., & Denisenkova, S. N. 1990, Soviet Astronomy Letters, 16, 275

DIERCKX, P. 1981, IMA Journal of Numerical Analysis, 1, 267, doi: 10.1093/imanum/1.3.267

Dotter, A., Chaboyer, B., Jevremović, D., et al. 2008, The Astrophysical Journal Supplement Series, 178, 89

D'Antona, F., Bellazzini, M., Caloi, V., et al. 2005, The Astrophysical Journal, 631, 868

Eddington, A. S. 1916, MNRAS, 77, 16, doi: 10.1093/mnras/77.1.16

Emden, R. 1907, Gaskugeln

Feiden, G. A., Skidmore, K., & Jao, W.-C. 2021, ApJ, 907, 53, doi: 10.3847/1538-4357/abcc03

Fontes, C. J., Zhang, H. L., Abdallah, J., J., et al. 2015, Journal of Physics B Atomic Molecular Physics, 48, 144014, doi: 10.1088/0953-4075/48/14/144014

Gratton, R., Sneden, C., & Carretta, E. 2004, ARA&A, 42, 385, doi: 10.1146/annurev.astro.42.053102.133945

Gratton, R. G., Carretta, E., & Bragaglia, A. 2012, Astronomy and Astrophysics Reviews, 20, 50, doi: 10.1007/s00159-012-0050-3

Gratton, R. G., Bonifacio, P., Bragaglia, A., et al. 2001, A&A, 369, 87, doi: 10.1051/0004-6361:20010144

Grevesse, N., & Sauval, A. J. 1998, SSRv, 85, 161, doi: 10.1023/A:1005161325181

Henyey, L. G., Forbes, J. E., & Gould, N. L. 1964, ApJ, 139, 306, doi: 10.1086/147754

Herschel, W. 1814, Philosophical Transactions of the Royal Society of London, 248

Huebner, W. F., & Barfield, W. D. 2014, Opacity, Vol. 402, doi: 10.1007/978-1-4614-8797-5

Husser, T. O., Wende-von Berg, S., Dreizler, S., et al. 2013, A&A, 553, A6, doi: 10.1051/0004-6361/201219058

Iglesias, C. A., & Rogers, F. J. 1996, ApJ, 464, 943, doi: 10.1086/177381

Jao, W.-C., Henry, T. J., Gies, D. R., & Hambly, N. C. 2018, ApJL, 861, L11, doi: 10.3847/2041-8213/aacdf6

Kovetz, A., Yaron, O., & Prialnik, D. 2009, MNRAS, 395, 1857, doi: 10.1111/j.1365-2966.2009.14670.x

Krishna Swamy, K. S. 1966, ApJ, 145, 174, doi: 10.1086/148752

Magee, N. H., Abdallah, J., J., Clark, R. E. H., et al. 1995, in Astronomical Society of the Pacific Conference Series, Vol. 78, Astrophysical Applications of Powerful New Databases, ed. S. J. Adelman & W. L. Wiese, 51

Magee, N. H., Abdallah, J., Colgan, J., et al. 2004, in American Institute of Physics Conference Series, Vol. 730, Atomic Processes in Plasmas: 14th APS Topical Conference on Atomic Processes in Plasmas, ed. J. S. Cohen, D. P. Kilcrease, & S. Mazavet, 168–179

Mansfield, S., & Kroupa, P. 2021, A&A, 650, A184, doi: 10.1051/0004-6361/202140536

Milone, A., Marino, A., Piotto, G., et al. 2012, The Astrophysical Journal, 745, 27

Milone, A. P., Piotto, G., Bedin, L. R., et al. 2012, ApJ, 744, 58, doi: 10.1088/0004-637X/744/1/58

Milone, A. P., Marino, A. F., Piotto, G., et al. 2015, ApJ, 808, 51, doi: 10.1088/0004-637X/808/1/51

Norris, J. 1987, The Astrophysical Journal, 313, L65

Nutzman, P., & Charbonneau, D. 2008, PASP, 120, 317, doi: 10.1086/533420

Osborn, W. 1971, The Observatory, 91, 223

Paxton, B., Bildsten, L., Dotter, A., et al. 2011, The Astrophysical Journal Supplement Series, 192, 3, doi: 10.1088/0067-0049/192/1/3

Piotto, G., Bedin, L. R., Anderson, J., et al. 2007, The Astrophysical Journal Letters, 661, L53, doi: 10.1086/518503

Plez, B. 2008, Physica Scripta Volume T, 133, 014003, doi: 10.1088/0031-8949/2008/T133/014003

Richardson, L. 2007, April

Roh, D.-G., Lee, Y.-W., Joo, S.-J., et al. 2011, ApJL, 733, L45, doi: 10.1088/2041-8205/733/2/L45

Seaton, M. J., Yan, Y., Mihalas, D., & Pradhan, A. K. 1994, MNRAS, 266, 805, doi: 10.1093/mnras/266.4.805

Stetson, P. B., & Harris, W. E. 1988, The Astronomical Journal, 96, 909, doi: 10.1086/114856

Tayar, J., Somers, G., Pinsonneault, M. H., et al. 2017, The Astrophysical Journal, 840, 17

van Saders, J. L., & Pinsonneault, M. H. 2012, ApJ, 751, 98, doi: 10.1088/0004-637X/751/2/98

Vinyoles, N., Serenelli, A. M., Villante, F. L., et al. 2017, The Astrophysical Journal, 835, 202

Virtanen, P., Gommers, R., Oliphant, T. E., et al. 2020, Nature Methods, 17, 261, doi: 10.1038/s41592-019-0686-2